Journal of Materials Chemistry B

PAPER

View Article Online
View Journal | View Issue

Cite this: J. Mater. Chem. B, 2019, 7, 3716

Stimuli-responsive local drug molecule delivery to adhered cells in a 3D nanocomposite scaffold†

Andisheh Motealleh,[a] Rossella De Marco[b] and Nermin Seda Kehr*[a]

Received 26th March 2019,
Accepted 9th May 2019

DOI: 10.1039/c9tb00591a

rsc.li/materials-b

Drug delivery systems capable of providing controlled and localized drug release are a highly important tool in the biomedical field because they can provide site-specific, sustained, and controlled drug release at the place where the drug is most needed, and they allow for significantly lower doses of the drug at other parts of the body, reducing the drug's potential side effects. In this respect, we describe pH-responsive PMO/alginate nanocomposite (NC) scaffolds with different pH-responsive strengths for controlled local drug delivery applications. To prepare the PMO/alginate NC scaffolds, PMOs were first loaded with anti-cancer molecules and then coated with a non-biopolymer or a biopolymer, after which the PMOs were embedded into an alginate network. We found that drug release from the PMOs was regulated by the pH of the environment and the surface coating of the PMOs due to the different pH-dependent levels of electrostatic interactions between all the charged components of the NC scaffolds. The non-biopolymer-coated formulation of the NC scaffold can be utilized to deliver higher dosages of drug molecules directly to cells, while the biopolymer-coated system is useful for slow and prolonged release of drugs and for enhanced cell adhesion. Nonetheless, both systems can be utilized, in particular, to deliver higher dosages of drug molecules directly to cancer cells while delivering less of the drug to healthy cells.

Introduction

Drug delivery systems capable of providing controlled and localized drug release, often called implantable drug delivery systems (IDDSs),[1,2] are a highly important tool in the biomedical field because they offer several advantages over conventional drug administration methods (*e.g.* the oral and parental route of drug administration). IDDSs have been designed to provide site-specific, sustained, and controlled drug release at the location where the drug is most needed in order to improve patient compliance and to allow for significantly lower doses of drug at other parts of the body, reducing the drug's potential side effects.[3,4] Furthermore, IDDSs allow for the delivery of drugs that cannot and/or should not be delivered *via* the oral route, due to their adsorption in the gastro-intestinal tract, highly toxic side effects, or because they would be more beneficial with site-specific dosing (*e.g.* anti-cancer drugs, steroids, antibiotics).

Nanocontainers and hydrogels represent excellent types of IDDSs due to their ability to provide biocompatibility, stability, controlled delivery, and biodegradability.[5–7] Hydrogels, which are crosslinked three-dimensional (3D) polymer networks, are widely used as 3D cell culture and drug delivery systems in tissue engineering and biomedical applications.[8–10] Hydrogels improve not only cell adhesion but also drug resistance, and they provide localized controlled drug delivery due to their bioadhesive characteristics, hydrophilic nature, injectability and 3D network.[11,12] Furthermore, polymer-based nanoparticles, *e.g.* polylactic-*co*-glycolic acid (PLGA) or polylactic acid (PLA), alginate, liposomes, micelles, and inorganic nanoparticles, have been intensively studied for their use as drug delivery vehicles. Among these, porous silica-based nanocontainers are promising candidates for controlled drug delivery applications due to their large surface area, narrow pore size distributions, and surfaces that are easy to functionalize.[13–19] Porous silica-based nanocontainers can encapsulate a wide variety of hydrophobic or hydrophilic (bio)molecules and protect them against chemical and biological degradations. Furthermore, simple surface modifications can improve their interaction with biological systems, reduce any associated harmful effects, and provide site-specific targeting.

Recent years have seen increased interest in the development of stimuli-responsive nanoparticle/hydrogel composite systems, namely nanocomposite (NC) hydrogels, which represent multifunctional biomaterials suitable for tissue engineering and local drug delivery applications.[20,21] For example, Lin *et al.*[22] described biocompatible LAPONITE® (LP)-embedded alginate hydrogels for pH-responsive cationic drug delivery. Gaharwar *et al.* reported κ-carrageenan-based hydrogels loaded with nanosilicates[23] and injectable stimuli-responsive magnetic nanoparticle-embedded

[a] Physikalisches Institut and Center für Soft Nanoscience, Westfälische Wilhelms-Universität Münster, Busso-Peus Straße 10, D-48149 Münster, Germany. E-mail: seda@uni-muenster.de
[b] Department of Chemistry "G. Ciamician", University of Bologna, via Selmi 2, 40126 Bologna, Italy

† Electronic supplementary information (ESI) available. See DOI: 10.1039/c9tb00591a

poly(*N*-isopropylacrylamide-*co*-acrylamide) (poly(NIPAM-*co*-AM)) hydrogels[24] for sustained release of therapeutic biomacromolecules. In such systems, the nanoparticle contribution to hydrogel network improves the mechanical properties of the hydrogel and increases biomolecule adsorption (*e.g.* proteins, growth factors) on the 3D network of the biomaterial due to nanoparticles' large surface areas; biomolecule adsorption thereby results in the sustained release of biomolecules and in enhanced cell adhesiveness and cell spreading.

In this context, we have previously reported on polyelectrolyte-coated zeolite L-embedded alginate hydrogels for pH-responsive controlled delivery of fluorescent dye molecules to adhered cells.[25] However, in that study, to be able to release the organic molecules from the zeolites L particles, the acidity of the cell culture media had to be changed by adding an acidic solution; this would clearly not be applicable in clinical situations. In another contribution, we described self-assembled monolayers (SAMs) of chiral periodic mesoporous organosilica (PMO) as a 2D platform for the pH-responsive delivery of fluorescent dye molecules and drug molecules to adhered healthy and cancer cells.[26] The SAMs of the chiral PMOs showed a greater amount of dye/drug molecules released in the presence of Colo 818 cancer cells than healthy fibroblast cells due to the local acidic environment of the cancer cells. In addition, we showed that the chirality of the PMOs influenced the amount of cells that adhered, therefore the released molecules, interacted with different amount of cells which allowing us to tune the extent of local drug delivery.

In this contribution, we aim to combine our previous studies to design a new NC hydrogel as a 3D platform for pH-responsive surface-mediated delivery of anti-cancer drug molecules targeted toward mostly cancer cells (and avoiding healthy cells). We prepared our pH-responsive NC hydrogel by first loading anti-cancer molecules into PMOs, then coating the loaded PMOs with poly-L-lysine (PLL), and finally embedding the coated and loaded PMOs into an alginate hydrogel network. The prepared pH-responsive PMO/alginate hydrogel showed prolonged release of a moderate and high dosage of drug molecules under physiological and acidic conditions (pH 6.0, simulating a tumor tissue environment), respectively due to the different pH-dependent levels of electrostatic interactions between the all charged components of the final NC hydrogel. Therefore, our pH-responsive PMO/alginate hydrogel was able to deliver locally more anti-cancer drug molecules to cancer cells than to healthy cells due to the local acidic environment generated by the cancer cells.

In this respect, this work has presented a novel strategy for designing anti-cancer drug-loaded, pH-sensitive NPs, and the resulting 3D NC hydrogels allow for stimuli-responsive local drug delivery and enhanced cancer therapy.

Experimental

Materials

Poly-L-lysine (PLL, MW: 30 000–70 000), poly(styrenesulfonate) (PSS), hexadecyltrimethylammonium bromide (CTAB, 98%), 1,2-bis(trimethoxysilyl)ethane (BTME, 96%), and trypsin were purchased from Sigma-Aldrich. Doxorubicin (DOX) was purchased from Sigma-Aldrich. Toluene, ethanol (absolute for analysis), ammonia solution (32%, pure) and hydrochloric acid (HCl) (32%, for analysis), were purchased from Merck. Glass plates (1.8 cm × 1.8 cm) were obtained from VWR. The cell medium (RPMI 1640) supplemented with 1% (v/v) penicillin/streptomycin, 2% L-glutamine, and 10% (v/v) fetal bovine serum (FBS) were obtained from Biochrom, Germany. Calcein AM (≥96.0% (HPLC)) and propidium iodide (≥94.0% (HPLC)) were purchased from Sigma-Aldrich. Primary dermal fibroblasts: normal, human, adult (ATCC® PCS-201-012™) cells were obtained from ATCC. Human Colo 818 (malignant melanoma) cells were purchased from DSMZ.

The detail information of how to synthesis the PMO-NH_2, and how to determine the amount of DOX in ^{DOX}PMO-NH_2 and later, ^{DOX}PMO-(PSS)PLL are mentioned in ESI.†

Loading of DOX into PMO-NH_2 (^{DOX}PMO-NH_2)

PMO-NH_2 (100 mg) was suspended in 1 mL water and mixed with 0.9 mM DOX. This reaction mixture was stirred for 1 day at room temperature. The final product ^{DOX}PMO-NH_2 was obtained by centrifugation, washed with water 1×, and dried at room temperature.

General procedure for preparing NC hydrogels of PMO-(PSS)PLL, ^{DOX}PMO-NH_2, and ^{DOX}PMO-(PSS)PLL

Stock solutions of alginate (1.25 g) in 100 mL double distilled water and calcium D-gluconate monohydrate (1.00 g) in 100 mL double distilled water were prepared. The suspension of PMO-PSS/PLL, ^{DOX}PMO-NH_2, and ^{DOX}PMO-PSS/PLL (1 mg) in calcium D-gluconate monohydrate (1 mL) was sonicated for 20 min and then added into the alginate solution (2 mL) during vortexing.

General procedure for preparing NC alginate scaffolds of PMO-(PSS)PLL, ^{DOX}PMO-NH_2, and ^{DOX}PMO-(PSS)PLL

The cross-linked NC alginate hydrogel of PMO-PSS/PLL, ^{DOX}PMO-NH_2, and ^{DOX}PMO-PSS/PLL (100 μL) was transferred into a Teflon container, frozen at −20 °C for 16 h and then lyophilized in a freeze dryer for 16 h.

DOX release from NC alginate scaffolds of ^{DOX}PMO-NH_2 and ^{DOX}PMO-(PSS)PLL at pH 7.4 and pH 6.0

NC scaffolds of ^{DOX}PMO-NH_2 and ^{DOX}PMO-(PSS)PLL (1 mg mL^{-1}) were suspended in cell culture media at pH 7.4 and in cell culture media at pH 6.0 (pH 6.0 was obtained by titration with hydrochloric acid 32 wt% in H_2O) and mixed at room temperature; DOX levels were measured at various time intervals. The fluorescence intensity of released DOX was measured from the supernatant taken from the sample. The amount of DOX released from NC scaffolds of ^{DOX}PMO-NH_2 and ^{DOX}PMO-(PSS)PLL at pH 7.4 and pH 6.0 was determined by using the formula from the calibration curve of different DOX concentrations: $y = 20\,224x + 10\,474$ (Fig. S1, ESI†).

General procedure for the cell experiments in NC alginate scaffolds of PMO-(PSS)PLL, ^{DOX}PMO-NH_2, and ^{DOX}PMO-(PSS)PLL

The healthy fibroblasts and Colo 818 cancer cells were carefully thawed and suspended in 10% FBS containing cell culture media (RPMI 1640). Then the cells (*ca.* 20 000) were separately seeded onto the NC alginate scaffolds of PMO-(PSS)PLL, ^{DOX}PMO-NH_2, and ^{DOX}PMO-(PSS)PLL, covered with the cell culture media at pH 7.4, and incubated for various time intervals (*e.g.* from 30 min to 14 days) at 37 °C and 5% CO_2. After the incubation periods, each of the NC scaffolds was washed twice with PBS to remove non-adhered cells. Subsequently, NC scaffolds were transferred to another cell culture plate and treated with EDTA (0.04% w/v in PBS, without Ca^{2+}/Mg^{2+}) with gentle mixing. The cells were counted immediately using a Neubauer chamber (trypan blue solution was used to detect dead cells).

General procedure for the PrestoBlue assay for cell proliferation and viability

The cell viability (%) was determined according to the PrestoBlue cell viability reagent protocol. For this measurement, scaffolds in the presence of cells were incubated for 2 hours, 1 day, 3 days and 7 days at 37 °C with 5% CO_2. After each incubation time, the scaffolds were washed with 1 mL PBS solution (2×) to remove unattached cells on scaffolds, then they were transferred to a new cell culture plate and dissolved with 50 μL EDTA (0.04% w/v in PBS, without Ca^{2+}/Mg^{2+}). The fresh media (200 μL) was added onto each scaffold and mixed with 20 μL per well PrestoBlue reagent. The samples were incubated for 1 h, then measured at 570 nm.

General procedure for the double staining of cells with calcein-AM and propidium iodide

Calcein AM/propidium iodide staining were employed to check the cellular viability or cell death, respectively. For this purpose 1 μM calcein AM and 1.5 μM Propidium Iodide were added at the same time into ^{DOX}PMO-(PSS)/PLL-Alg and ^{DOX}PMO-NH_2-Alg scaffolds in presence of fibroblast and colo 818 cells (after 7 days of incubation), the samples were kept in incubator at 37 °C and 5% CO_2 for 30 min, then they were checked by fluorescence microscope.

Characterization

The morphology of the PMOs was investigated with scanning electron microscopy (SEM) using a Zeiss 1540 EsB dual beam focused ion beam/field emission scanning electron microscope. Zeta potential measurements and dynamic light scattering (DSL) were done with a Malvern Zetasizer Nano Series. The rheological behaviour of each sample was provided by Anton Paar Rheometer. The ANOVA test was used for statistical analyses. A spectrofluorometer (Fluorolog Horiba Jobin Yvon) was used to determine the amount of DOX in the PMOs. The occupancy rate of the hydrogels (how much of the hydrogel surface area was taken up by the PMOs) was determined using ImageJ software. A time-resolved spectrofluorometer (Fluorolog Horiba Jobin Yvon) was used to determine the calibration curve for different concentrations of DOX (emission maximum = 550 nm).

Results and discussion

Preparation of pH responsive PMOs

Synthesis of ^{DOX}PMO-NH_2 and ^{DOX}PMO-(PSS)PLL were described previously by us (for details see the ESI†).[26] Briefly, we first synthesized amino-functionalized PMOs (PMO-NH_2) and loaded them with the anti-cancer drug DOX to obtain ^{DOX}PMO-NH_2. The drug loading and the encapsulation efficiency of doxorubicin in ^{DOX}PMO-NH_2 were 44.3%, and 88.6%, respectively, and these values for ^{DOX}PMO-(PSS)PLL were 43.8% and 87.6%, respectively (for details see the ESI†). The prepared PMO-NH_2 and ^{DOX}PMO-NH_2 were coated with oppositely charged polyelectrolytes (PSS and PLL) according to the layer-by-layer (LbL) deposition technique to obtain PMO-PSS/PLL (as a control) and ^{DOX}PMO-PSS/PLL, respectively and to increase the pH responsiveness of the DOX release from PMOs. Subsequently, we determined the adsorbed amount of polymers onto the PMO-NH_2 and ^{DOX}PMO-NH_2 by using UV/Vis spectrophotometry (Table S1, ESI†). The content of drug molecules (DOX) in the pores of ^{DOX}PMO-NH_2 and ^{DOX}PMO-PSS/PLL was determined using fluorescence spectrometry (Fig. S1 and Table S2, ESI†). Almost the same amount of PSS/PLL was adsorbed onto the PMO-NH_2 and ^{DOX}PMO-NH_2. The content of DOX loaded into the ^{DOX}PMO-PSS/PLL and ^{DOX}PMO-NH_2 was almost same.

The prepared PMO-PSS/PLL, ^{DOX}PMO-NH_2, and ^{DOX}PMO-PSS/PLL were characterized by dynamic light scattering (DLS), scanning electron microscopy (SEM) and zeta-potential. The size of the PMOs increased after PSS/PLL coating, shown by DLS (Table S3, ESI†). The SEM images show the spherically shaped ^{DOX}PMO-NH_2, PMO-PSS/PLL, and ^{DOX}PMO-PSS/PLL (Fig. 1). The change in the zeta potential was observed after PSS/PLL coating of (PMO-NH_2/^{DOX}PMO-NH_2), demonstrating the successful coating of PMO-NH_2/^{DOX}PMO-NH_2 with PSS/PLL (see Table S4 for zeta potential data for each coating, ESI†).

Preparation of NC scaffolds of ^{DOX}PMO-NH_2 and ^{DOX}PMO-(PSS)PLL and determining the release of DOX from the respective pH-responsive NC scaffolds

PMO-PSS/PLL, ^{DOX}PMO-NH_2 and ^{DOX}PMO-PSS/PLL were embedded into an alginate hydrogel network and freeze-dried to obtain pH-responsive NC scaffolds (PMO-(PSS)PLL-Alg, ^{DOX}PMO-NH_2-Alg, and ^{DOX}PMO-(PSS)PLL-Alg). The prepared NC scaffolds were

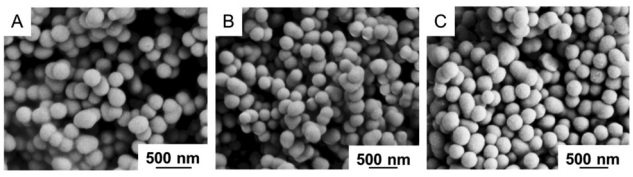

Fig. 1 SEM images of ^{DOX}PMO-NH_2 (A) PMO-(PSS)PLL (B) and ^{DOX}PMO-(PSS)PLL (C).

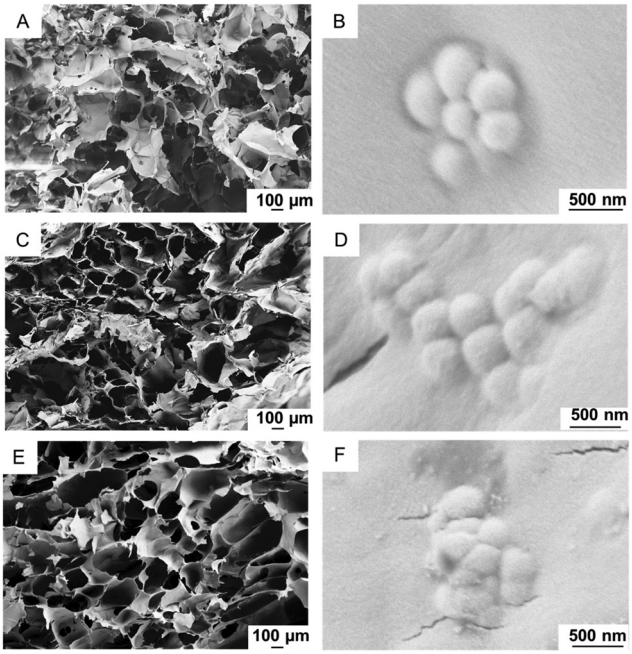

Fig. 2 SEM images of NC hydrogels of (A) PMO-(PSS)PLL-Alg and (B) its focus image, (C) ^{DOX}PMO-NH_2-Alg and (D) its focus image, (E) ^{DOX}PMO-(PSS)PLL-Alg and (F) its focus image. (B, D and F) Are showing the respective PMOs in the PMO-(PSS)PLL-Alg, ^{DOX}PMO-NH_2-Alg, and ^{DOX}PMO-(PSS)PLL-Alg.

analysed by different techniques to determine their morphological, swelling, degradation, porosity, and rheological, properties (Fig. 2 and Fig. S2, S3, Tables S5–S9, ESI†).

The 3D porous alginate scaffold network and the embedded PMOs in the alginate scaffold wall can be seen in the SEM images (Fig. 2). The PMO distribution on a 1 μm^2 area of each scaffold was determined by ImageJ's multi-point tool using SEM images of the respective NC scaffolds (Table S5, ESI†). The quantitative amount of ^{DOX}PMO-NH_2 and ^{DOX}PMO-PSS/PLL were almost the same in the respective scaffolds, as measured with fluorescence spectrometry (Table S6, ESI†). The swelling ratio, degradation behaviour, and porosity of the ^{DOX}PMO-NH_2-Alg and ^{DOX}PMO-PSS/PLL-Alg scaffolds were determined and compared with alginate scaffolds alone to investigate the impact of PMOs (Tables S7–S9, ESI†). In general, larger pores and/or higher porosity can store more water or (bio)molecules, but they can also result in decreased stability. However, the PMO-embedded scaffolds exhibited a higher swelling capacity, higher porosity, and less degradation in comparison to the alginate scaffold alone, showing that the incorporation of hydrophilic porous PMOs into the alginate scaffold enhances the hydrophilicity and mechanical stability of the network. Rheology measurements were done for Alg and ^{DOX}PMO-NH_2-Alg, and ^{DOX}PMO-(PSS)PLL-Alg hydrogel. G' and G'' were done under constant oscillation conditions (Fig. S2 and S3, ESI†). G' or the storage modulus demonstrates elastic stress, G'' or loss modulus displays viscous stress and apparent viscosity (μ) as a function of angular frequency. The results showed that alginate hydrogel with presence of PMOs had more viscose structure than alginate hydrogel itself (Fig. S2, ESI†), because PMOs serve as cross-linkers like described previously.[27] Therefore, the NC hydrogel had stronger network which produced higher storage modulus (Fig. S3, ESI†). By adding PMO within hydrogel network the storage modulus (G') and the loss modulus (G'') were increased. G' was much more than G'' which proves that the alginate hydrogel and PMO alginate hydrogel are viscoelastic gels. Furthermore, we observed that ^{DOX}PMO-(PSS)PLL-Alg gave higher values of G' and G'' than the ^{DOX}PMO-NH_2-Alg. This data indicating that the electrostatic interaction between ^{DOX}PMO-(PSS)PLL and Alg resulted in a stronger gel structure.

The DOX release kinetics from ^{DOX}PMO-NH_2-Alg and ^{DOX}PMO-PSS/PLL-Alg was investigated at different incubation time periods at pH 7.4 and pH 6.0 (Fig. 3, 4 and Tables S10, S11, ESI†). The initial burst release of DOX from ^{DOX}PMO-NH_2-Alg and ^{DOX}PMO-PSS/PLL-Alg at pH 7.4 was about 23% and 15.0% within the first 5 h (Fig. 3, 4 and Tables S10, S11, ESI†). On the other hand, at pH 6.0, we observed a higher initial burst release of DOX from ^{DOX}PMO-NH_2-Alg and ^{DOX}PMO-PSS/PLL-Alg (around 32% and 28%, respectively), during the same period. The release profiles of DOX from ^{DOX}PMO-NH_2-Alg and ^{DOX}PMO-PSS/PLL-Alg at pH 7.4 and 6.0 show a sustained and extended release pattern (Fig. 3) after 5 h incubation. We observed that more of the drug was released from ^{DOX}PMO-NH_2-Alg and ^{DOX}PMO-PSS/PLL-Alg at an acidic pH value, which is representative of a tumor tissue environment, than at pH 7.4 in all incubation periods. For example, after 30 days, at pH 7.4 and at pH 6.0, ^{DOX}PMO-NH_2-Alg/^{DOX}PMO-PSS/PLL-Alg released 42%/29% and 66%/50% of the DOX, respectively (Fig. 4 and Table S11, ESI†). This means 1.6/1.7 times more DOX was released from ^{DOX}PMO-NH_2-Alg/^{DOX}PMO-PSS/PLL-Alg at pH 6.0 than at pH 7.4. In addition, after the same incubation period, we investigated that at pH 7.4 and 6.0, almost 1.5/1.3 times more DOX was released from ^{DOX}PMO-NH_2-Alg in comparison with ^{DOX}PMO-PSS/PLL-Alg (Fig. 4 and Table S11, ESI†) showing that the amount of drug released from the PMOs depends on pH of the release environment and the surface coating of PMOs

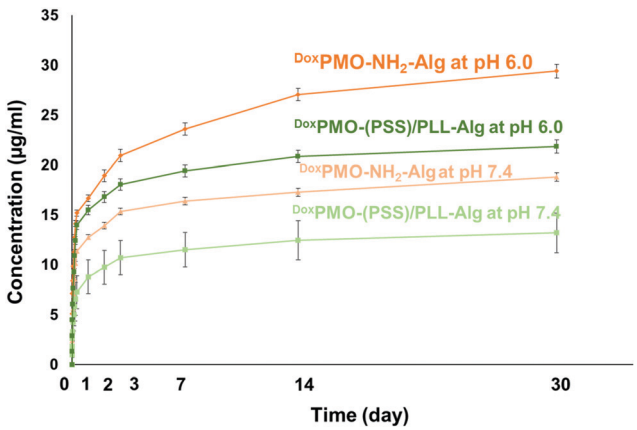

Fig. 3 The amount of DOX (μg mL^{-1}) released from the ^{DOX}PMO-NH_2-Alg and ^{DOX}PMO-(PSS)/PLL-Alg scaffold over different time intervals at pH 7.4 and pH 6.0 (N = 6); data show significant differences; ANOVA: $p < 0.05$ for all data.

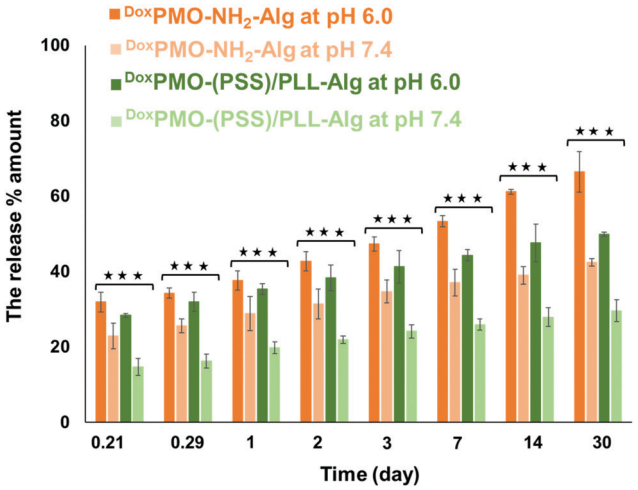

Fig. 4 The amount of DOX (in percentage) released from ^{DOX}PMO-NH_2-Alg (orange), and ^{DOX}PMO-(PSS)/PLL-Alg (green), at pH 7.4 (light color) and 6.0 (dark color) after 30 days [number of experiments (N) = 3; data show significant differences; ANOVA: $p < 0.001$ (***)].

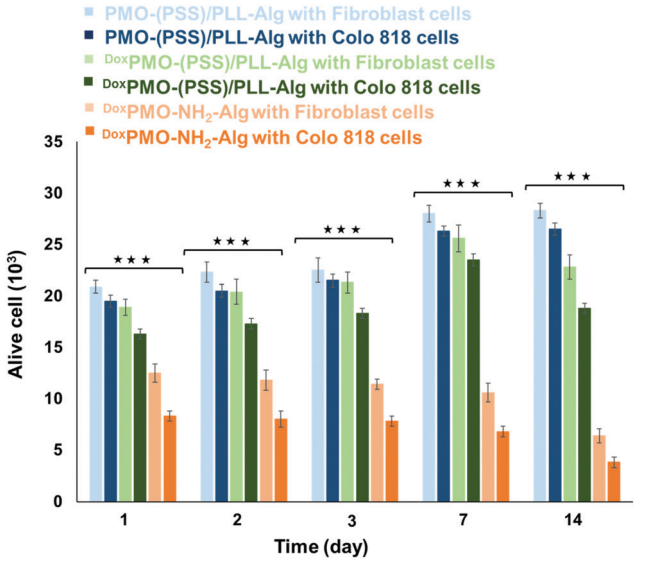

Fig. 5 The adhered amount of alive fibroblasts (light color) and Colo 818 (dark color) cells ($\times 10^3$) on PMO-(PSS)/PLL-Alg (blue), ^{DOX}PMO-(PSS)/PLL-Alg (green), and ^{DOX}PMO-NH_2-Alg (orange) at different incubation time periods [number of repeated experiments (N) = 6; data show significant differences; ANOVA: $p < 0.001$ (***)].

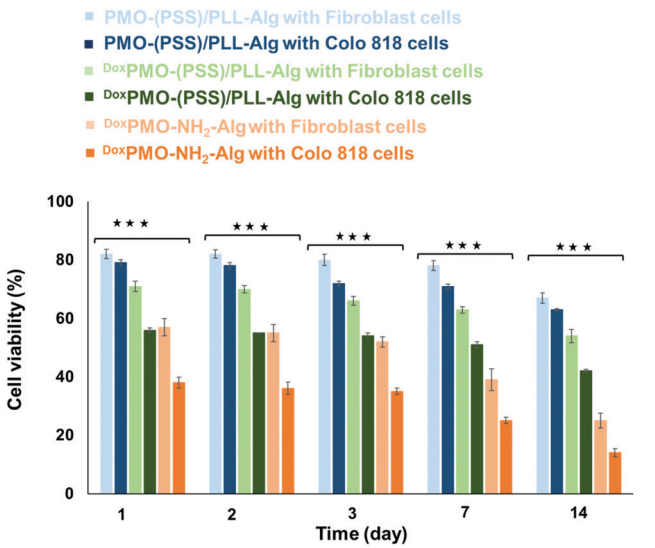

Fig. 6 The cell viability (%) of fibroblasts (light color) and Colo 818 (dark color) cells on PMO-(PSS)/PLL-Alg (blue), ^{DOX}PMO-(PSS)/PLL-Alg (green), and ^{DOX}PMO-NH_2-Alg (orange) at different incubation time periods [number of repeated experiments (N) = 6; data show significant differences; ANOVA: $p < 0.001$ (***)].

with polyelectrolytes, which considerably slowed the release rate of DOX.

Alginate has been used successfully for the entrapment and/or delivery of a variety of (bio)molecules, *e.g.* drugs, proteins, and for the development of a controlled drug delivery system.[18,28] In our system the positively charged functional group on ^{DOX}PMO-NH_2 and ^{DOX}PMO-PSS/PLL (DOX, NH_2, PLL) can interact with the carboxyl groups in alginate and ultimately form DOX|Alg, DOX|PMO-NH_2|Alg and DOX|PMO-PSS/PLL|Alg complexes, and the release of DOX from such composite hydrogel complexes become sustained and pH dependent as the degradation of the hydrogel proceeds and the electrostatic interactions between the charged components change. Specifically, our pH-responsive ^{DOX}PMO-NH_2-Alg and ^{DOX}PMO-PSS/PLL-Alg allowed us to achieve prolonged release of DOX and a prolonged release of a high dosage of DOX under physiological and acidic conditions, respectively, that can be also regulated *via* the polyelectrolyte coating on the PMOs.

Surface-mediated pH-responsive delivery of DOX to cancer and healthy cells in NC scaffolds

Cell experiments were performed in the respective NC hydrogels to study surface-mediated pH-controlled delivery of anti-cancer drug molecules to cancer cells and healthy cells in a 3D matrix of PMO-PSS/PLL-Alg, ^{DOX}PMO-NH_2-Alg and ^{DOX}PMO-PSS/PLL-Alg. PMO-PSS/PLL-Alg was used as a control to analyse the effect of DOX on cell viability.

Primary healthy fibroblasts and malignant Colo 818 cells (20 000 cells) were separately seeded into PMO-PSS/PLL-Alg, ^{DOX}PMO-NH_2-Alg and ^{DOX}PMO-PSS/PLL-Alg and incubated for various time intervals (30 min to 14 days) at 37 °C in cell culture media at pH 7.4. After each incubation time, the number of alive adherent cells and the cell viability in each of the scaffolds were determined (Fig. 5, 6 and Table S12, ESI†).

We observed that DOX had a negative effect on cell viability already at the beginning of the experiment (Fig. 5, 6 and Table S12, ESI†). After only 30 min incubation (Table S12, ESI†), the viability of healthy cells (fibroblasts) and cancer cells (Colo 818) reduced to 75%/60% and 81%/76% in ^{DOX}PMO-NH_2-Alg and ^{DOX}PMO-PSS/PLL-Alg, respectively. On the other hand, the viability of cells in PMO-PSS/PLL-Alg was 93% (fibroblasts) and 84% (Colo 818). Longer incubation times resulted in further decreases in cell viability in each of the scaffolds (Fig. 6), but, interestingly, the opposite trend was observed for the number of alive cells in

PMO-PSS/PLL-Alg and ^{DOX}PMO-PSS/PLL-Alg (Fig. 5). After 14 days of incubation, the number of cells in PMO-PSS/PLL-Alg and ^{DOX}PMO-PSS/PLL-Alg increased (Fig. 5 and Table S12, ESI†), although the cell viability was reduced (Fig. 6 and Table S12, ESI†). Importantly, the number of alive cells and the cell viability was (fibroblast/Colo818) less in ^{DOX}PMO-PSS/PLL-Alg than in PMO-PSS/PLL-Alg due to the toxic effects of DOX.[29] On the other hand, we observed a decrease both in the alive cell content and cell viability in ^{DOX}PMO-NH_2-Alg scaffold. We found, *e.g.*, 3.5 times more alive fibroblast cells and 2.2 times greater fibroblast cell viability in ^{DOX}PMO-PSS/PLL-Alg than ^{DOX}PMO-NH_2-Alg after 14 days of incubation. These results indicate that the biopolymer coating at the PMO surfaces enhanced cell growth. This means that while DOX causes cell death, the PLL-coated PMO surfaces support cell proliferation within the respective incubation periods.

More interestingly, we observed a considerable difference in cell viability between fibroblast and Colo 818 cells in ^{DOX}PMO-NH_2-Alg and ^{DOX}PMO-PSS/PLL-Alg scaffolds that was more pronounced after 2 days of incubation (Fig. 6 and Table S12, ESI†). The cancer cell (Colo 818) viability was *ca.* 19%/15% less than that of the healthy cells (fibroblasts) in ^{DOX}PMO-NH_2-Alg and ^{DOX}PMO-PSS/PLL-Alg scaffolds. We attribute this difference to the local acidic environment of the cancer cells, which initiated the release of higher amounts of DOX from the pH-responsive ^{DOX}PMO-NH_2 and ^{DOX}PMO-PSS/PLL than was initiated in comparison to the healthy cell environment.

On the other hand, when we consider the numbers of alive cancer cells and healthy cells, we recognized a significant difference between ^{DOX}PMO-NH_2-Alg and ^{DOX}PMO-PSS/PLL-Alg scaffolds (Fig. 5 and Table S12, ESI†). While an ~18% difference was observed in the number of alive cancer cells and healthy cells in ^{DOX}PMO-PSS/PLL-Alg, a 41% difference was found in ^{DOX}PMO-NH_2-Alg after 14 days of incubation. This means that the difference between the cell proliferation rate and the cell death rate in ^{DOX}PMO-NH_2-Alg was less significant than in ^{DOX}PMO-PSS/PLL-Alg, resulting in fewer alive cells with lower cell viability in ^{DOX}PMO-NH_2-Alg yet higher numbers of alive cells with lower cell viability in ^{DOX}PMO-PSS/PLL-Alg.

In order to strengthen these results, we used the PrestoBlue metabolic assay to monitor cell proliferation and cell viability in PMO-PSS/PLL-Alg, ^{DOX}PMO-NH_2-Alg and ^{DOX}PMO-PSS/PLL-Alg for different incubation times (Fig. 7, 8 and Tables S13, S14, ESI†). The results showed a continuous decrease in metabolic activity and viability as a function of incubation time in ^{DOX}PMO-NH_2-Alg. On the other hand, we determined an increase in cell proliferation in PMO-PSS/PLL-Alg and ^{DOX}PMO-PSS/PLL-Alg even though there was also a continuous decrease in cell viability, which was more pronounced in ^{DOX}PMO-PSS/PLL-Alg than PMO-PSS/PLL-Alg.

Furthermore we used fluorescence microscopy to determined cell viability (Fig. 9 and 10) qualitatively. Since DOX was internalized into the cells, dead cells was visualized by microscope in red color and alive cells without color and by overlapping the images, it was possible to determine the amount of alive cells and dead cells at the same time. The double staining (alive/dead) cell was also done which is shown in Fig. 10. Calcein AM and propidium iodide were used as an additional tool to show the ratio between alive and dead cells, respectively.

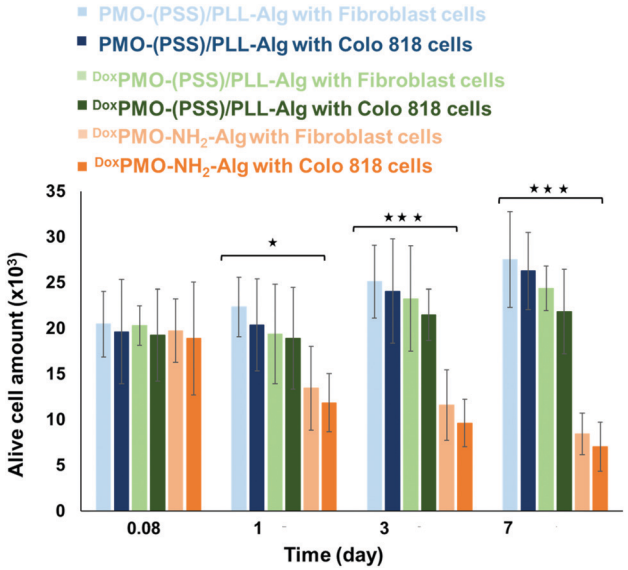

Fig. 7 The amount of alive cells ($\times 10^3$) of fibroblasts (light color), and Colo 818 (dark color) in PMO-(PSS)/PLL-Alg (blue), ^{DOX}PMO-(PSS)/PLL-Alg (green), and ^{DOX}PMO-NH_2-Alg, (orange), and at different incubation time periods determined by the PrestoBlue assay [number of repeated experiments (N) = 6; data show significant differences; ANOVA: $p < 0.05$ (*), $p < 0.01$ (**), $p < 0.001$ (***)].

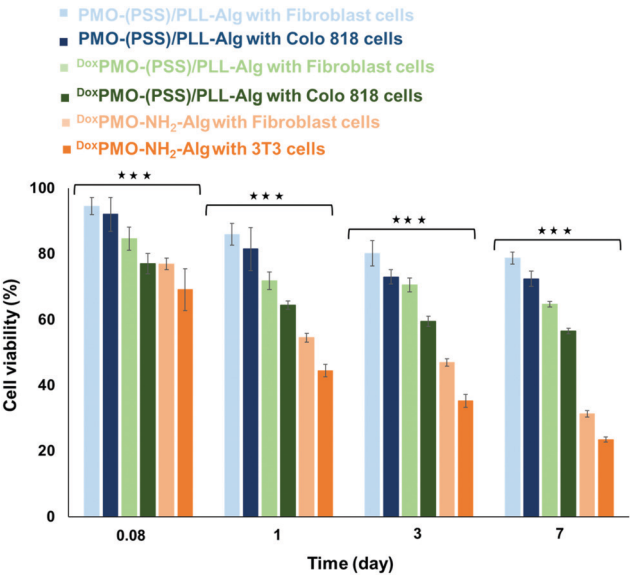

Fig. 8 The cell viability (%) of fibroblasts (light color), and Colo 818 (dark color) cells in PMO-(PSS)/PLL-Alg (blue), ^{DOX}PMO-(PSS)/PLL-Alg (green), and ^{DOX}PMO-NH_2-Alg, (orange) at different incubation time periods determined by the PrestoBlue assay and a hemocytometer. [Number of repeated experiments (N) = 6; data show significant differences; ANOVA: $p < 0.001$ (***)].

Thus, these complementary results demonstrate that both systems, ^{DOX}PMO-NH_2-Alg and ^{DOX}PMO-PSS/PLL-Alg, can be

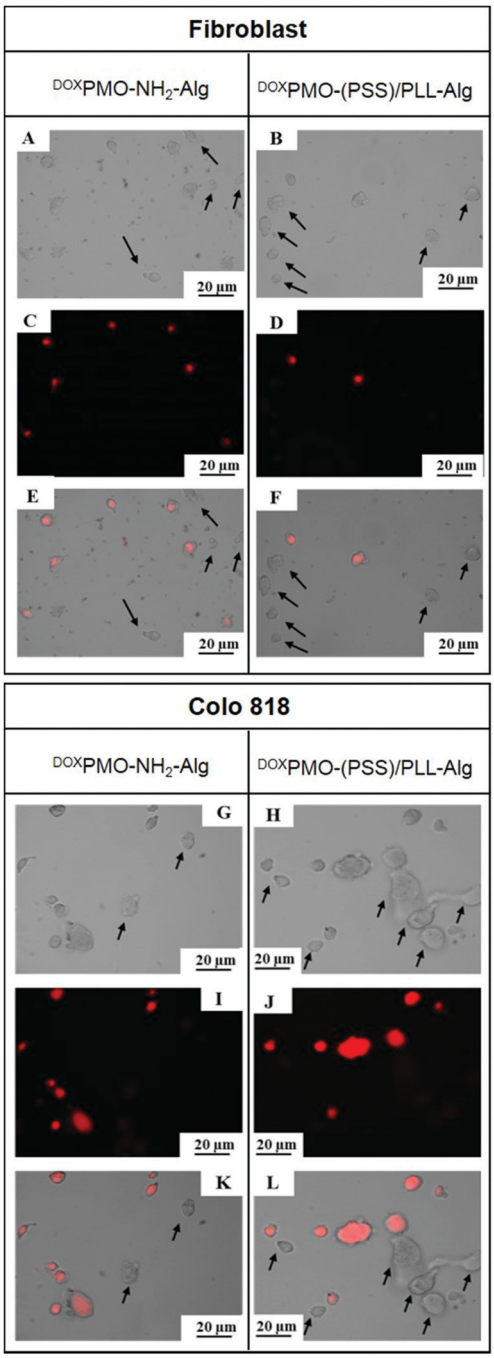

Fig. 9 Fibroblasts (A–F) and Colo 818 (G–L) cells within ^{DOX}PMO-(PSS)/PLL-Alg and ^{DOX}PMO-NH_2-Alg scaffolds at 40× magnification (red: dead cells by doxorubicin) after 7 days of incubation time (the arrows show the alive cells).

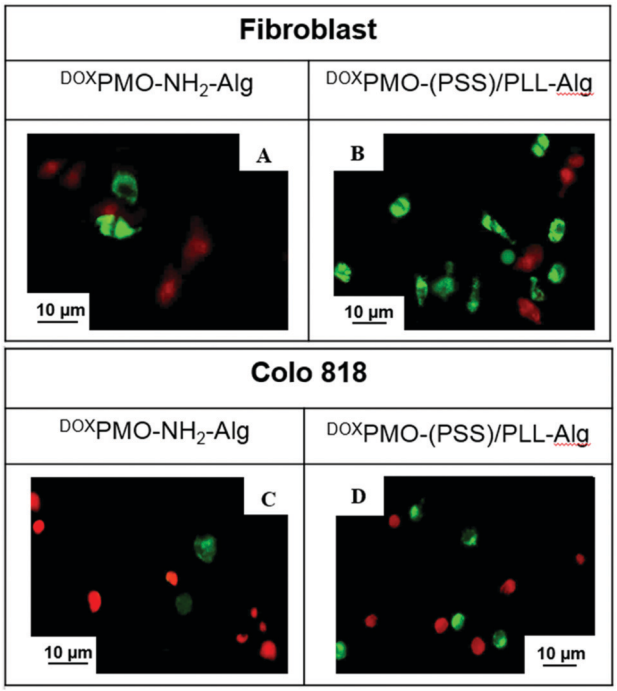

Fig. 10 Fibroblasts (A and B) and Colo 818 (C and D) cells within ^{DOX}PMO-(PSS)/PLL-Alg and ^{DOX}PMO-NH_2-Alg scaffolds at 40× magnification (red: dead cells by Propidium Iodide, green: alive cells by calcein AM) after 7 days of incubation time.

used for different purposes. ^{DOX}PMO-PSS/PLL-Alg is the most suitable system when the goal is to enhance cell proliferation within the 3D biomaterial network and to have a slow drug release rate; conversely, ^{DOX}PMO-NH_2-Alg should be used when the purpose is to administer fast and high dosage therapy. Furthermore both systems are suitable for affecting/damaging cancer cells more than healthy cells when the cells have the same exposure time to the drug.

Conclusions

In this study, we presented the preparation of pH-responsive NC scaffolds ^{DOX}PMO-NH_2-Alg and ^{DOX}PMO-PSS/PLL-Alg, that showed sustained and extended release of the DOX from PMOs at pH 7.4 and pH 6.0. The respective cell experiments within ^{DOX}PMO-NH_2-Alg and ^{DOX}PMO-PSS/PLL-Alg demonstrated an improved cell adhesion in ^{DOX}PMO-PSS/PLL-Alg than ^{DOX}PMO-NH_2-Alg and a decrease in cell viability in both systems, whereby there was a positive effect of the biopolymer at the PMO surfaces on cell proliferation and a toxic effect of DOX on the cells. Furthermore, we determined a difference in cell viability between healthy cells and cancer cells due to the high dosage release of DOX under acidic pH conditions than physiological conditions. Therefore, we found less viability for cancer Colo 818 cells than healthy fibroblasts due to the local acidic environment of the Colo 818 cancer cells.

Overall, these results demonstrate that our pH-responsive ^{DOX}PMO-NH_2-Alg and ^{DOX}PMO-PSS/PLL-Alg can potentially be used in local drug delivery applications. ^{DOX}PMO-NH_2-Alg can be utilized in particular to deliver higher dosages of drug molecules directly to cells, while ^{DOX}PMO-PSS/PLL is useful for slow and prolonged release of drugs and for enhanced cell adhesion. Nonetheless, both systems can be utilized to deliver high dosages of drug molecules directly to cancer cells while delivering less of the drug to healthy cells.

For future work, we will work on to increase the number of polymer layer on PMOs and to increase the cross-linking density of alginate to have a better control on the drug

molecules release and to slow down the initial burst release of drug molecules.

Conflicts of interest

There are no conflicts to declare.

Acknowledgements

We thank Deutsche Forschungsgemeinschaft [DFG (award number: KE 1577/7-2)] for funding and Dr Celeste Riley Brennecka for scientific editing.

Notes and references

1 B. P. Timko and D. S. Kohane, *Isr. J. Chem.*, 2013, **53**, 728.
2 A. N. Zelikin, *ACS Nano*, 2010, **4**, 2494.
3 Y. Liu, H. L. Liu, J. Sun, L. L. Sang and H. C. Xu, *J. Biomater. Tissue Eng.*, 2015, **5**, 323.
4 E. M. M. del Valle, M. A. Galán and R. G. Carbonell, *Ind. Eng. Chem. Res.*, 2009, **48**, 2475.
5 S. Mura and J. Nicolas, *Nat. Mater.*, 2013, **12**, 991.
6 Y. J. Zhu and F. Chen, *Chem. – Asian J.*, 2015, **10**, 284.
7 S. Naahidi, M. Jafari, F. Edalat, K. Raymond, A. Khademhosseini and P. Chen, *J. Controlled Release*, 2013, **166**, 182.
8 A. Peppas, J. Z. Hilt, A. Khademhosseini and R. Langer, *Adv. Mater.*, 2006, **18**, 1345.
9 B. V. Slaughter, S. S. Khurshid, O. Z. Fisher, A. Khademhosseini and N. A. Peppas, *Adv. Mater.*, 2009, **21**, 3307.
10 A. Khademhosseini and R. Langer, *Biomaterials*, 2007, **28**, 5087.
11 N. A. Peppas, P. Bures, W. Leobandung and H. Ichikawa, *Eur. J. Pharm. Biopharm.*, 2000, **50**, 27.
12 N. A. Peppas and J. J. Sahlin, *Biomaterials*, 1996, **17**, 1553.
13 W. Feng, X. Zhou, C. He, K. Qiu, W. Nie, L. Chen, H. Wang, X. Mo and Y. Zhangab, *J. Mater. Chem. B*, 2013, **1**, 5886.
14 S. Girat, M. W. Chi Man and C. Carcel, *Chem. – Eur. J.*, 2015, **21**, 13850.
15 D. Tarn, C. E. Ashley, M. Xue, E. C. Carnes, J. I. Zink and C. J. Brinker, *Acc. Chem. Res.*, 2013, **46**, 792.
16 K. N. Yang, C. Q. Zhang, W. Wang, P. C. Wang, J. P. Zhou and X. J. Liang, *Cancer Biol. Med.*, 2014, **11**, 34.
17 Q. L. Li, Y. Sun, Y. L. Sun, J. Wen, Y. Zhou, Q. M. Bing, L. D. Isaacs, Y. Jin, H. Gao and Y. W. Yang, *Chem. Mater.*, 2014, **26**, 6418.
18 C. Gao, F. Tang, G. Gong, J. Zhang, M. P. M. Hoi, S. M. Y. Lee and R. Wang, *Nanoscale*, 2017, **9**, 12533.
19 J. I. Kwon, C. M. Lee, H. S. Jeong, P. S. Oh, H. Hwang, S. T. Lim, M. H. Sohn and H. J. Jeong, *Nucl. Med. Mol. Imaging*, 2015, **49**, 312.
20 A. Motealleh and N. S. Kehr, *Adv. Healthcare Mater.*, 2017, **6**, 1600938.
21 A. K. Gaharwar, N. A. Peppas and A. Khademhosseini, *Biotechnol. Bioeng.*, 2014, **111**, 441.
22 Y. Li, D. Maciel, H. Tomás, J. Rodrigues, H. Ma and X. Shi, *Soft Matter*, 2011, **7**, 6231.
23 G. Lokhande, J. K. Carrow, T. Thakur, J. R. Xavier, M. Parani, K. J. Bayless and A. K. Gaharwar, *Acta Biomater.*, 2018, **70**, 35.
24 N. A. Jalili, M. K. Jaiswal, C. W. Peak, L. M. Cross and A. K. Gaharwar, *Nanoscale*, 2017, **9**, 15379.
25 B. Ergün, L. De Cola, H. J. Galla and N. S. Kehr, *Adv. Healthcare Mater.*, 2016, **5**, 1588.
26 A. Motealleh, P. Dorri and N. S. Kehr, *J. Mater. Chem. B*, 2019, **7**, 2362–2371.
27 N. S. Kehr, E. A. Prasetyanto, K. Benson, B. Ergün, A. Galstyan and H. J. Galla, *Angew. Chem., Int. Ed.*, 2013, **52**, 1156.
28 L. Chen, R. Shen, S. Komasa, Y. Xue, B. Jin, Y. Hou, J. Okazaki and J. Gao, *Int. J. Mol. Sci.*, 2017, **18**, 989.
29 O. Tacara, P. Sriamornsakb and C. R. Dassa, *J. Pharm. Pharmacol.*, 2013, **65**, 157.